AAPS PharmSciTech (© 2018)
DOI: 10.1208/s12249-018-0952-0

Research Article

Improving Properties of Albendazole Desmotropes by Supramolecular Systems with Maltodextrin and Glutamic Acid

Agustina Bongioanni,[1,2] Bruno Sousa Araújo,[3] Yara Santiago de Oliveira,[4] Marcela R. Longhi,[1,2] Alejandro Ayala,[3] and Claudia Garnero[1,2,5]

Received 18 October 2017; accepted 2 January 2018

Abstract. Albendazole, an effective broad-spectrum anthelmintic agent, showed unpredictable therapeutic response caused by poor water solubility and slow dissolution rate. Then, novel binary and multicomponent supramolecular systems of two different solid forms of albendazole (I and II) with maltodextrin alone or with glutamic acid were studied as an alternative to improve the oral bioavailability of albendazole. The interactions and effects on the properties of albendazole were studied in solution and solid state. The solid systems were characterized using Raman and Fourier transform-infrared spectroscopy, thermal analysis, powder X-ray diffraction, and scanning electron microscopy. The solubility measurements, performed in aqueous and simulated gastric fluid, showed that albendazole (form II) was the most soluble form, while its supramolecular systems showed the highest solubility in simulated gastric fluid. On the other hand, the dissolution profiles of binary and multicomponent systems in simulated gastric fluid displayed pronounced increments of the dissolved drug and a faster dissolution rate compared to those of free albendazole forms. Thus, these supramolecular structures constitute an interesting alternative to improve the physicochemical properties of albendazole, with potential application for the preparation of pharmaceutical oral formulations.

KEY WORDS: albendazole; desmotrope; maltodextrin; glutamic acid; solubility; dissolution.

INTRODUCTION

It is well known that active pharmaceutical ingredients (APIs) can exist in different crystalline solid forms. This phenomenon, known as polymorphism, can produce significant changes in their chemical and physical properties including solubility, stability, bioavailability, and organoleptic characteristics, among others (1,2). The relevance of controlling polymorphism in the pharmaceutical industry is associated with its significant impact on the preformulation research, which is of great significance for the rational design of novel materials with optimal quality, safety, and efficacy.

Albendazole (ABZ, Scheme 1) is an effective broad-spectrum anthelmintic agent (3). This benzimidazole carbamate, used in human and veterinary medicine (4–6), showed unpredictable therapeutic response due to low and erratic oral bioavailability caused by poor water solubility and slow dissolution rate. Also, two solid forms have been described for ABZ, designated as ABZI and ABZ (7,8). In our previous report, the desmotropy of ABZ has been studied revealing different tautomeric states in solid state (7).

Different approaches have been previously investigated to improve the solubility, the dissolution rate, and/or the bioavailability of ABZ, including liposome, solid dispersions, microencapsulation, co-crystallization, microcrystal formulation, nanoparticles, and complexes with cyclodextrins (9–11). However, only our recent study has considered the different solid forms of this API. We have reported novel complexes of forms I and II of ABZ with β-cyclodextrin (β-CD) as an alternative to improve the oral bioavailability of ABZ (12).

Recently, maltodextrins (MDs, Scheme 1) have been successfully used for drug delivery (13–15). MDs are products obtained from the partial hydrolysis of food grade starch with suitable acids and/or enzymes, which consist of a mixture of

Electronic supplementary material The online version of this article (https://doi.org/10.1208/s12249-018-0952-0) contains supplementary material, which is available to authorized users.

[1] Departamento de Ciencias Farmacéuticas, Facultad de Ciencias Químicas, Universidad Nacional de Córdoba, Córdoba, Argentina.
[2] Unidad de Investigación y Desarrollo en Tecnología Farmacéutica—UNITEFA (CONICET-UNC), Córdoba, Argentina.
[3] Departamento de Física, Universidade Federal do Ceará, Fortaleza, Ceara, Brazil.
[4] Departamento de Farmácia, Universidade Federal do Ceará, Fortaleza, Ceara, Brazil.
[5] To whom correspondence should be addressed. (e–mail: garneroc@fcq.unc.edu.ar)

Published online: 20 February 2018

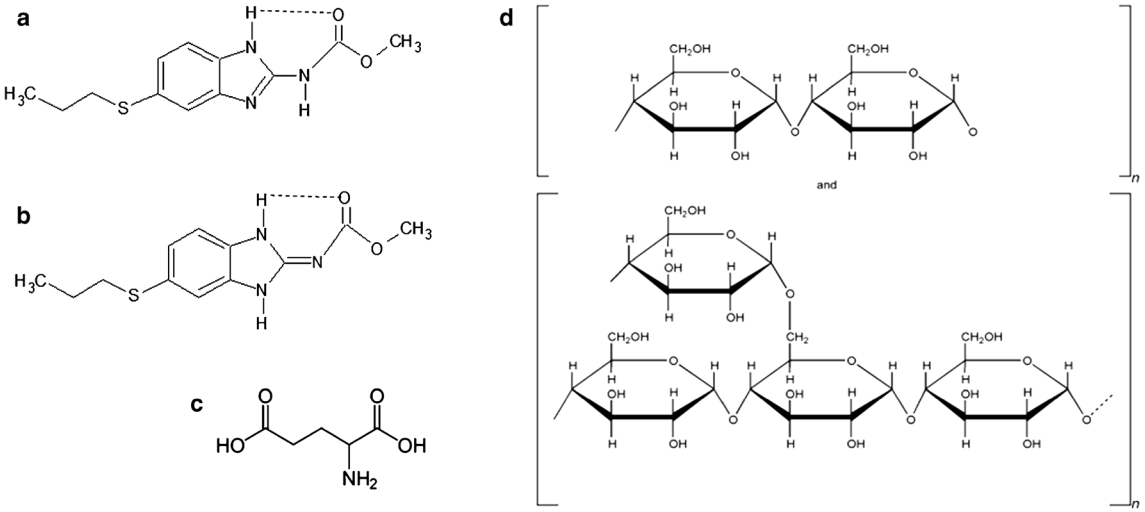

Scheme 1. (a) ABZI, (b) ABZII, (c) GLU and (d) MD

saccharide polymers (amylose and amylopectin). In addition, the formation of multicomponent complexes with a specifically selected third auxiliary substance has become more frequent in order to improve the desired physicochemical, chemical, or toxicological properties of different APIs (16,17). In particular, some aminoacids have been used as third components to increase the aqueous solubility of APIs (16,18,19).

In this work, we focused our interest on the study of supramolecular binary complexes of forms I and II of ABZ with MD. In addition, multicomponent complexes were obtained considering the basic nature of ABZ by adding glutamic acid (GLU, Scheme 1), an acid aminoacid, as third component. We prepared and characterized the complexes, evaluating their effect on the solubility and dissolution behavior of the two solid forms of ABZ.

MATERIAL AND METHODS

Chemicals and Reagents

Albendazole (ABZ) and maltodextrin (MD, MW = 10,370) were provided by Todo Droga (Argentina). L-glutamic acid (GLU) was supplied by Anedra (Argentina), while *potassium bromide* was purchased from Merck (Germany). Methanol, analytical reagent grade, was obtained from Cicarelli (Argentina). A Millipore Milli Q Water Purification System (Millipore, Bedford, MA, USA) generated the water used in these studies. All other chemicals were of analytical grade.

Obtaining the Form II of Albendazole

The solid form II of ABZ was recrystallized from a methanol solution as previously reported (10). ABZ form I that corresponds to the commercially available ABZ was dissolved in methanol, heated, and stirred until a clear solution was formed. Then, the solution was filtered, followed by slow evaporation of the solvent under ambient conditions until crystallization was complete. Light brown crystals were collected after 10 days.

Solubility Studies

The effects of MD alone or with GLU on the solubility of forms I and II of ABZ were studied in aqueous and simulated gastric fluid without enzymes (SFG). The solubility measurements were performed according to the method of Higuchi and Connors (20). An excess of ABZ (approximately 20 mg of forms I and II, respectively) was added to solutions containing increasing concentrations of MD, which ranged from 0.9 to 9.5 mM. In the presence of GLU, an excess of ABZ was added to solutions containing MD ranging from 0.9 to 9.5 mM and GLU 7.5 mM. The suspensions were agitated in an ultrasonic bath (Elmasonic S40) and then maintained at 37.0 ± 0.1°C for 72 h in a constant-temperature water bath (Pilot One, Huber). After that, the remaining solid ABZ was removed by filtration through a 0.45-μm membrane filter (Millipore, USA). The clear solutions were suitably diluted and analyzed by UV-Vis spectrophotometry (Agilent Cary 60 spectrophotometer).

Preparation of Solid Samples

Solid-state binary and multicomponent systems of ABZI and ABZII in equimolar ratio with the ligands were prepared as follows:

Kneading Method (KN)

The systems ABZI:MD (KNB-I), ABZII:MD (KNB-II), ABZI:MD:GLU (KNT-I), and ABZII:MD:GLU (KNT-II) were prepared by accurately weighing appropriate amounts of MD and then transferring them to a mortar. A methanol-water (50:50, *v/v*) mixture was added to the MD powder and the resultant slurry was kneaded for about 10 min. Then, the corresponding solid form of ABZ was added in small portions with the simultaneous addition of the solvent in order to maintain a suitable consistency. For multicomponent systems, GLU was added simultaneously. These slurries were kneaded thoroughly for about 45 min, and the resultant pastes were dried in vacuum at 45°C for 72 h, and protected from light.

Physical Mixture (PM)

Physical mixtures of ABZI:MD (PMB-I), ABZII:MD (PMB-II), ABZI:MD:GLU (PMT-I), and ABZII:MD:GLU (PMT-II) were prepared by simply blending the corresponding components uniformly with a mortar and pestle.

Raman Spectroscopy

Raman spectra were recorded on a LabRAM HR (Horiba) spectrometer equipped with a liquid N2-cooled CCD detector using a near infrared laser (785 nm) for excitation, with a power of 100 mW. The spectral region studied was 50–4000 cm^{-1} and the measurements were carried out using a ×50 nir microscope objective, with an acquisition time of 150 s by region.

Fourier Transform-Infrared Spectroscopy (FT-IR)

The FT-IR spectra were recorded on a Nicolet 5 SXC FT-IR Spectrophotometer (Madison, WI, USA), with the potassium bromide disks being prepared by compressing the powder.

Thermal Analysis

Simultaneous differential scanning calorimetry (DSC) and thermogravimetric analysis (TGA) experiments were performed on a Jupiter STA 449 F3 Jupiter (Netzsch) system. Measurements were obtained over a temperature range of 30–450°C using a heating rate of 10°C min^{-1} and a sealed aluminum crucible with pierced lids containing 5 mg of sample. The sensors and the crucibles were under a constant flow of nitrogen (70 mL/min) during the experiment.

Powder X-Ray Diffraction (PXRD)

Powder X-ray diffraction patterns were obtained at ambient temperature using a Philips PW1710 diffractometer operating at 45 kV and 30 mA with Cu-Kα radiation. The powder pattern was collected by scanning 2θ from 2° to 40° with a step size of 0.05° at a scanning rate of 2.5 s/step.

Scanning Electron Microscopy Studies (SEM)

Microscopic morphological structures of the raw materials and the solid-state systems were investigated and photographed using a Carl Zeiss Σigma scanning electron microscope. The samples were fixed on a brass stub using a double-sided aluminum tape, which were gold-coated under vacuum by employing a sputter coater Quorum 150 to improve the conductivity.

Dissolution Studies

The dissolution profiles of the systems KNB-I, KNB-II, KNT-I, KNT-II, PMB-I, PMB-II, PMT-I, and PMT-II were evaluated in a dissolution apparatus (Hanson SR II 6 Flask Dissolution Test Station, Hanson Research Corporation, Chatsworth, CA, USA) using the paddle method according to USP apparatus 2, at a temperature of 37.0 ± 0.5°C and stirring at 50 rpm. Samples of each powder containing about 50 mg of ABZ were compressed using a hydraulic press at an appropriate force to obtain discs, which will not be disintegrated under the test conditions. The discs were immersed into 500 mL of SGF and aliquots of the dissolution medium were taken at appropriate time intervals, with immediate replacement by equal volumes of fresh medium maintained at the same temperature. Each sample was filtered, adequately diluted with dissolution media, and analyzed for ABZ content by spectrophotometry (Agilent Carry 60 spectrophotometer) at 299 nm. Cumulative percentages of the API released from the discs were calculated. All the experiments were performed in triplicate. The results were expressed as mean % of ABZ released (± SD) at the given sampling time.

The dissolution profiles were evaluated using the similarity factor (f2) (21), which is a model adopted by several guidances as a criterion for estimating the closeness between *in vitro* dissolution profiles (22) as:

$$f2 = 50\log\left\{\left[1+\frac{1}{n}\sum_{t=1}^{n}(R_t-T_t)^2\right]^{-0,5}100\right\} \quad (1)$$

where n is the number of sampling points, and R_t and T_t are the percentages dissolved of the reference and the test product, respectively, at each time point t. For curves to be considered similar, the f2 values should be close to 100. Generally, f2 values are greater than 50 (between 50 and 100), which implies an average difference of no more than 10% at the sample time points. This ensures equivalence of the two curves and, thus, of the performance of the test and the reference products.

RESULTS

Phase Solubility Analysis

The effect of MD and GLU on the solubility of both solid forms of ABZ was evaluated in aqueous and SGF solutions at 37.0 ± 0.1°C. Figure 1 shows the phase solubility diagrams obtained by plotting the changes in ABZ solubility as a function of MD concentration. All solubility profiles were classified according to Higuchi and Connors (20) (Table I). The apparent stability constant (KC) values were used to compare the affinity of the API for the ligands. The values, shown in Table I, were estimated from the slope of the initial linear portion of the diagrams and the intrinsic solubility of each solid form (S0), according to the following equation:

$$KC = \text{slope}/S0\,(1-\text{slope}) \quad (2)$$

Solid-State Characterization

In order to characterize samples prepared by the methods KN and PM, the solid samples were examined using several experiments such as Raman and FT-IR spectroscopy, DSC, TGA, PXRD, and SEM. Also, they were then

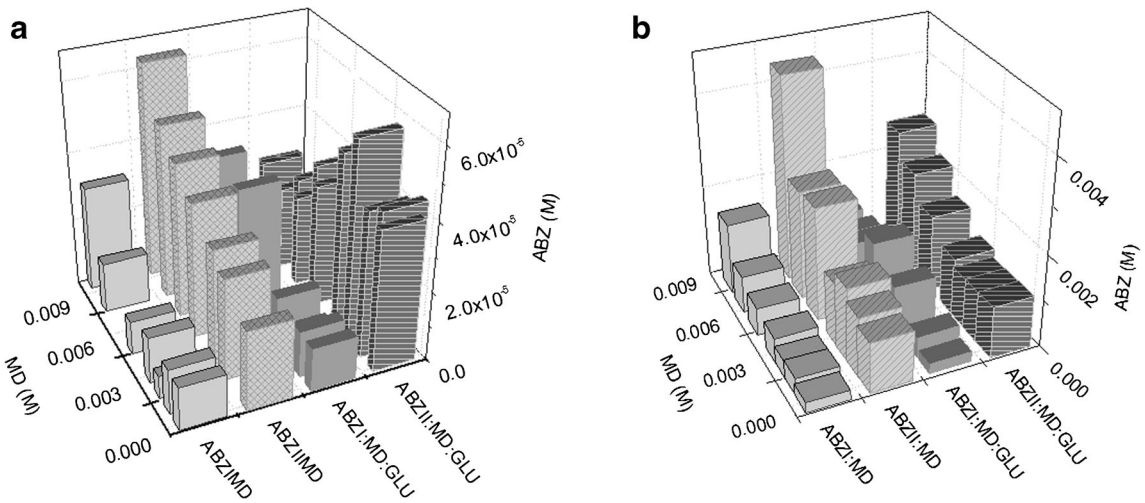

Fig. 1. Effect of MD and GLU on the solubility of ABZI and ABZII in **a** aqueous and **b** simulated gastric fluid solutions

compared to the pure components trying to obtain supporting evidence of interaction.

Raman Spectroscopy

It was possible to identify and unequivocally distinguish the solid forms I and II of ABZ from their Raman spectra. As depicted in Fig. 2b, ABZ I and ABZ II, in particular, exhibited significant spectral differences in the 150–800 cm^{-1} zone. Furthermore, differences were observed in the spectral region between 1300 and 1400 cm^{-1}. Additionally, with the aim of evaluating the effect of the procedure used for the preparation of solid binary and multicomponent systems, both ABZ forms were kneaded (ABZI KN, ABZII KN) for about 45 min. Both spectra were analyzed (Fig. 2b) and no differences were detected with respect to the spectra of the unprocessed samples.

Raman spectra of KNs and PMs systems were taken and compared with those of their corresponding free components: ABZI, ABZII, MD, and GLU (see Supplementary Material, Fig. S1). The spectra for KNs and PMs consisted of an overlay of the characteristic peaks of the pure compounds spectra.

FT-IR Spectroscopy

Segments of the FT-IR spectra of ABZI, ABZII, MD, GLU, and their corresponding KNs and PMs systems were evaluated (shown in Supplementary Material, Fig. S2). Both ABZ solid forms were characterized previously (7). Their FT-IR spectra revealed marked differences that allowed the distinction between both forms. The bands originated due to the NH stretching vibration could not be analyzed because they overlapped with the band attributed to the O–H stretching vibrations of MD. The FT-IR spectrum of KNB-II showed that the bands at 522 and 447 cm^{-1} shifted to higher frequencies. On the other hand, in the spectrum of KNT-I, it can be observed that the bands at 1442 and 1322 cm^{-1} disappeared. In the case of KNB-I, KNT-II, PMB-I, PMB-II, PMT-I, and PMT-II, the FT-IR spectra showed the superposition of the single components.

Thermal Analysis

The DSC and TGA profiles of ABZI, ABZII, MD, GLU, and their corresponding KNs and PMs systems are shown in Fig. 3. The DSC profile of ABZI showed three transitions: a melting

Table I. Summary of solubility studies at 37.0 ± 0.1°C

System	Smax (μg/mL)	Solubility Increased (S_{max}/S_0)	Kc (M^{-1})	Isotherm
Water				
ABZI:MD	9.9 ± 1.0	2.5	–	–
ABZI:MD:GLU	8.8 ± 1.3	2.7	105	AP
ABZII:MD	16.7 ± 1.8	2.8	324	AL
ABZII:MD:GLU	15.2 ± 0.3	2.5	–	B
Simulated gastric fluid				
ABZI:MD	416.1 ± 18.4	7.1	411	AP
ABZI:MD:GLU	356.5 ± 50.6	6.1	1373	B
ABZII:MD	1187.9 ± 21.5	4.0	309	AP
ABZII:MD:GLU	750.8 ± 44.9	2.5	120	AP

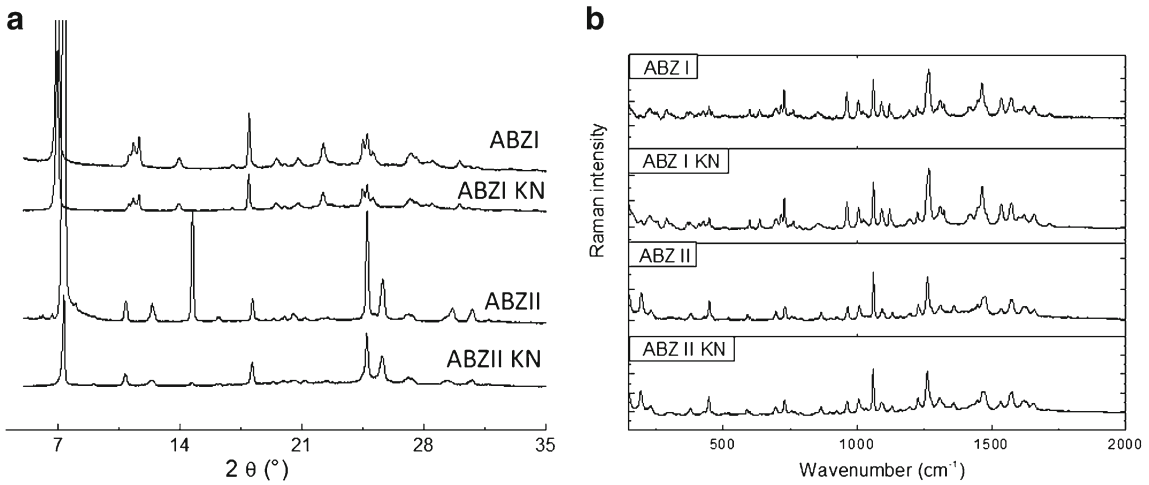

Fig. 2. **a** Powder X-ray diffraction patterns and **b** Raman spectra of ABZI, ABZI KN, ABZII, and ABZII KN

endotherm at 214.4°C (with onset at 194.4°C) with a weight loss of 12.4% in TGA and two endotherms at 323.5 and 378°C due to the decomposition phenomena which were associated with a mass loss of 39% beginning at 286°C. The DSC profile of ABZII showed four transitions: a weak endotherm at 158.6°C without mass loss over the range 130–180°C in the TGA curve, an endotherm at 215.2°C (with onset at 202.7°C) associated with a mass loss of 13% in TGA, and two exotherms at 320.4 and 379.7°C which were attributed to the decomposition of the drug, with a mass loss of 40.5% beginning at 290°C. This indicated a polymorphic phase transition, where form II transforms into form I and then melts as form I. On the other hand, the DSC trace of MD showed a broad endotherm with a maximum at about 99.3°C, corresponding to a dehydration process as determined by a mass loss of 4.36% registered by TGA as well as an endotherm at 237.1°C and an exotherm at 312.1°C, which were ascribed to the decomposition process due to their correlation with a mass loss of 56.84% in the TGA curve. The DSC curve obtained for GLU exhibited two main events: a sharp endothermic peak at 210.7°C (with onset at 206°C) attributable to the melting of the drug, with a mass loss of 12.8% in TGA, followed by a small exotherm at 314.3°C associated with the decomposition with a mass loss of 45.4%.

The DSC curves of binary KN systems displayed endotherms similar to those observed for the ABZ melting events, which could reflect the presence of remaining drug crystals unincorporated in the carrier. The profile of KNT-I showed endotherms only at 105.4 and 216.5°C, while the curve of PMT-I evidenced the characteristic events (118.9, 204.8, and 215.8°C) of the individual components. A similar behavior was found for KNB-II, which exhibited two endotherms at 137.4 and 215.9°C, while its corresponding PM reflected the presence of the individual components. In contrast, the curve of KNT-II was very similar to that of PMT-II.

In addition, a mass loss associated with the degradation phenomena was registered by TGA. The profiles showed that the decomposition of KNB-I, KNT-I, KNB-II, and KNT-II started above 208, 195, 183, and 203°C, respectively.

PXRD

The diffractograms shown in Fig. 4 were obtained from powder samples in order to investigate the characteristics of the obtained binary and ternary systems. In the PXRD patterns for both ABZ solid forms reported previously (7), diffractograms of crystalline compounds were evidenced. Clear differences in intensity and sharp peaks confirmed that they were different crystal forms. The diffractogram of MD showed a characteristic hollow pattern revealing its amorphous state, whereas GLU exhibited characteristic peaks consistent with its crystalline state. The PXRD patterns for KNs and MPs of binary and ternary systems displayed reflection characteristics of the components, according to each case, with intensities lower than those of pure materials.

Additionally, the effect of the procedure used for the preparation of solid binary and multicomponent systems was evaluated. Therefore, both ABZ free forms were kneaded (ABZI KN, ABZII KN) for about 45 min. The diffractograms were analyzed (Fig. 2a) and no differences were detected with respect to the patterns of the unprocessed samples.

SEM

Figure 5 illustrates the SEM photomicrographs showing the morphological differences between the samples. In our previous reports, ABZ I and II (12) showed a crystalline structure and MD (23) presented hollow spherical entities; while, in this work, GLU exhibited plate-like crystals. The SEM images of KN systems showed a drastic change in the morphology; it was observed that the original shape of the single materials disappeared. The KN systems showed a less ordered structure constituted by irregular compact particles with some cracks and small spherical slits. In particular, the slits were observed in greater quantity and definition in the ternary KNs. On the other hand, the raw materials were clearly detectable in the SEM images of PMs.

Dissolution Studies

Figure 6 shows the effect of the supramolecular binary and multicomponent systems on dissolution profiles in SFG. The f2 values are given in Table II.

In particular, the curves of the multicomponent systems of ABZI showed that the addition of GLU to the binary systems led to an increase in the percentage of dissolution of the API. It was determined that KNB-I produced a 66% of

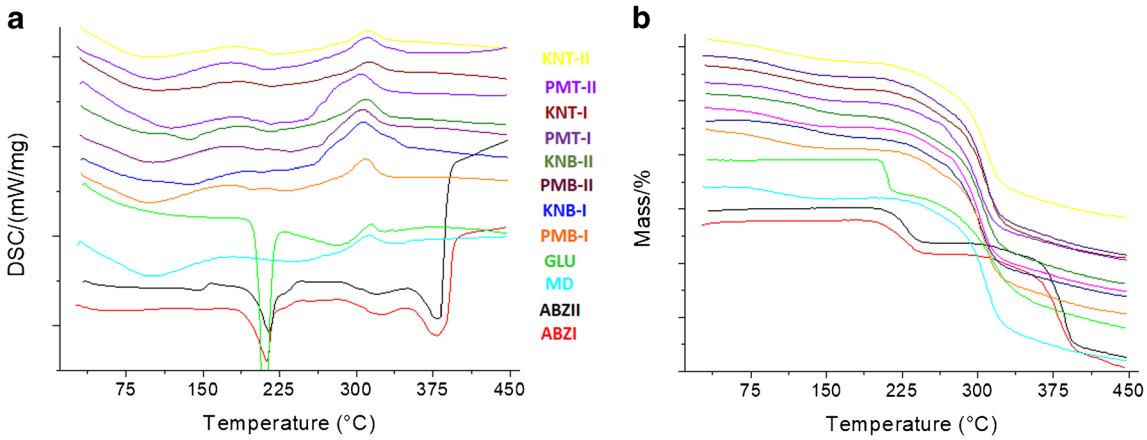

Fig. 3. **a** DSC and **b** TGA curves of ABZI, ABZII, MD, GLU, and binary and multicomponent systems

the drug dissolved, while KNT-I increased to 87%. PMB-I dissolved 65% of the API and PMT-I increased to 98%, while ABZI alone dissolves only 1.2%. On the other hand, the addition of GLU to the binary systems of ABZII did not show important modifications in the dissolution performance. The quantity of API dissolved after 120 min was as follows: 84% for KNB-II, 86% for KNT-II, 95% for PMB-II, and 100% for PMT-II, whereas ABZII alone dissolves only 1.3%. It was determined that PMT produced the highest dissolved percentage for both ABZ forms.

In addition, the dissolution profiles of the binary and multicomponent systems were compared with those of reference (free ABZI and ABZII, respectively) by applying the similarity factor (f2) (Table II).

DISCUSSION

Solubility Studies

ABZ is an API weakly basic in nature (pKa values of 2.68 and 11.83) categorized as class II in the biopharmaceutical classification system (24). Also, it is almost insoluble in water; its solubility decreases with increasing solution pH. In our previous report, the intrinsic solubility of ABZI and ABZII was determined (12). Hence, the complex formation appears as an especially effective strategy to improve the physicochemical properties of ABZ. Thus, the effect of MD and GLU on the solubility of both solid forms was evaluated in aqueous and SGF solutions at 37.0 ± 0.1°C.

According to the KC values (Table I), it can be observed that the ABZ ionization in SGF increased the interaction between each desmotrope and the ligands; consequently, the binary and multicomponent systems showed higher solubility. The KC values clearly demonstrated that, within experimental error, ABZI had higher affinity for the ligands than ABZII. However, ABZII:MD and ABZII:MD:GLU showed the highest solubility in SGF.

Although the binary and multicomponent complexes obtained with MD and GLU showed a significant increase in ABZ solubility, the amount solubilized was small in comparison with the solubility obtained with β-CD complexes (12).

Solid-State Characterization

In the present study, the characterization of the supramolecular systems has been addressed in great detail. However, the Raman and FT-IR spectra did not show significant differences between KN and PM evidencing the presence of more or less intense solid-state interactions

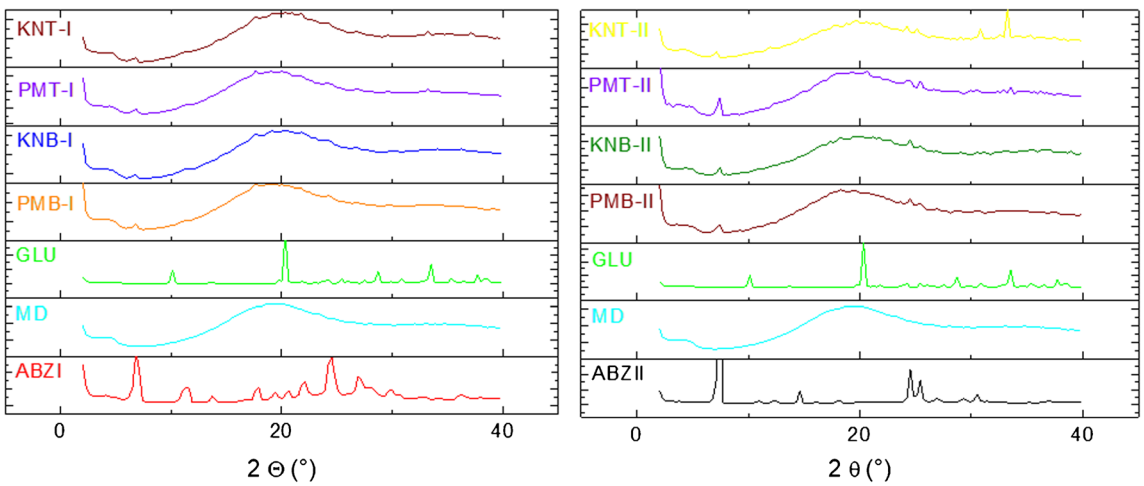

Fig. 4. Powder X-ray diffraction patterns of ABZI, ABZII, GLU, MD, ABZI:MD, ABZII:MD, ABZI:MD:GLU, and ABZII:MD:GLU systems

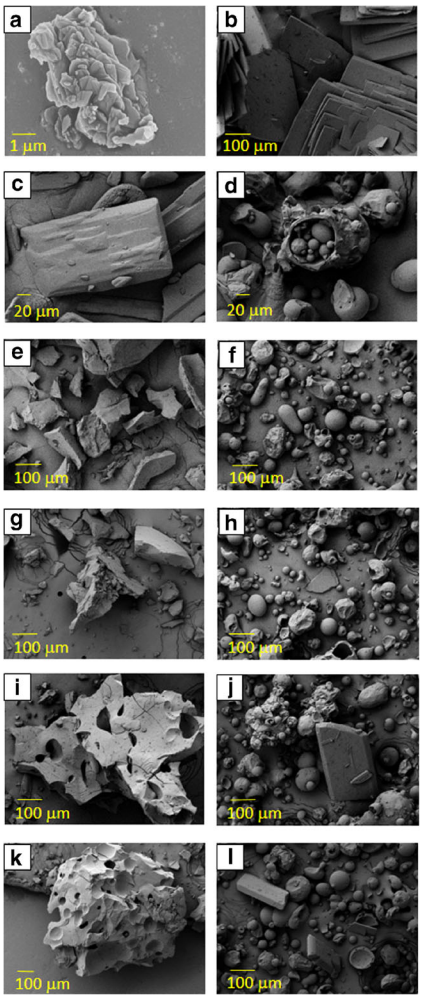

Fig. 5. SEM microphotographs of: **a** ABZI, **b** ABZII, **c** GLU, **d** MD, **e** KNB-I, **f** PMB-I, **g** KNB-II, **h** PMB-II, **i** KNT-I, **j** PMT-I, **k** KNT-II, and **l** PMT-II

between the components. Therefore, these techniques provide insufficient information to detect solid-state interactions in these systems.

Thus, another alternative methods was used. The results obtained by thermal analysis, PXRD, and SEM indicated molecular interactions in these supramolecular systems. The comparison of the thermal events of the binary and ternary systems prepared by KN with those obtained by PM revealed their different behavior, which demonstrates the interaction between components. Interestingly, the dehydration process determined in the TGA profiles of KNB-I and PMB-I revealed a mass loss of 6.3 and 7.2%, respectively, suggesting that most of the water molecules in MD helix were displaced by drug molecules in the KN system. Such thermal behavior showed structural differences between KN and PM, suggesting an interaction between the components of KN, as a likely inclusion process. Moreover, the mass loss value, associated with the degradation phenomena, revealed that KNB-I and KNT-II are the systems with higher thermal stability. Additionally, the diffractograms of the supramolecular systems showing broader and more diffused characteristic peaks revealed a decrease in their degree of crystallinity, in this way suggesting that ABZ could be included in the helix of MD. In addition, microscopic aspects and supporting evidence of the interaction between both solid ABZ forms and the ligands were obtained. The SEM photomicrographs of KN systems showing alterations in the shape and aspect of the particles suggested the formation of new solid phases, while the images of PMs confirmed the presence of crystalline particles and the absence of interactions.

Dissolution Studies

Poorly water-soluble drugs exhibit characteristics that are problematic for effective oral delivery such as rate-limiting dissolution, slow and erratic absorption, and low and variable bioavailability. In this context, enhancement of the dissolution rate in biological fluids is the first objective in the delivery of poorly soluble drugs like ABZ. Therefore, in our previous report, complexes of β-CD with both ABZ forms have demonstrated the ability to increase their dissolution performance (12). It was determined that the β-CD systems obtained by KN produce the highest dissolved percentage (65%) for ABZII. Whereas, the dissolution profiles of these novel systems with MD and GLU revealed significantly higher increases in the rate and percentage of dissolution, with a dissolution rate faster than that of the free

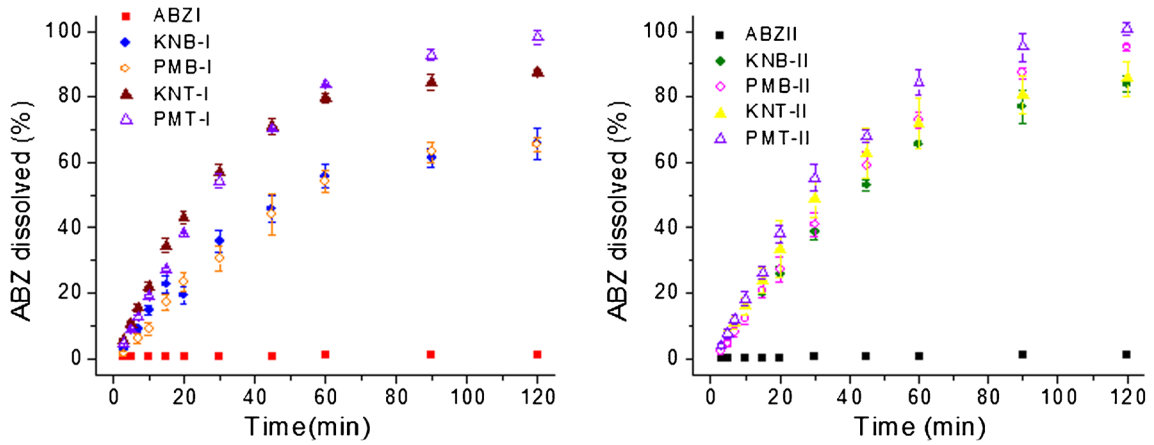

Fig. 6. Dissolution profiles in simulated gastric fluid of ABZI, ABZII, ABZI:MD, ABZII:MD, ABZI:MD:GLU, and ABZII:MD:GLU systems

Table II. Similarity factor (f2) of dissolution profiles

System	KNB-I	PMB-I	KNT-I	PMT-I	KNB-II	PMB-II	KNT-II	PMT-II
f2	19	23	12	17	16	17	14	18

solid forms. The significant dissolution enhancement that occurred with KNs may be attributed to both an increase of solubility upon complexation and a decrease of the crystalline state, as confirmed by PXRD. However, PMT produced the highest dissolved percentage for both ABZ forms. This effect can be related with an *in situ* solubilizing and wettability process, indicating that the presence of the ligands has significantly increased the dissolution of ABZ at stomach pH.

In addition, comparison of the dissolution profiles of supramolecular systems with those of reference (free ABZI and ABZII, respectively) was realized by applying the similarity factor (f2). The f2 values calculated were much lower than 100 (Table II), which indicated that the profiles of KNs and PMs were not similar to those of the free ABZ forms. These results demonstrated that the systems resulting from the interaction with the ligands produce a significant improvement in the dissolution rate of both ABZ forms.

CONCLUSIONS

The present work was able to demonstrate that novel systems of ABZ with MD alone or with GLU constitute new solid forms capable of improving the physicochemical properties of both ABZ solid forms. Spectroscopic techniques were considered minor and insufficient for determination of significant differences between KNs and PMs; therefore, the characterization of ABZI:MD, ABZII:MD, ABZI:MD:GLU, and ABZII:MD:GLU with thermal, X-ray, and microscopic methods was accomplished. The capacity of binary and multicomponent systems to improve solubility was demonstrated. In particular, ABZII:MD and ABZII:MD:GLU showed the highest solubility in SGF. Furthermore, the increase in ABZ solubility favored its dissolution in SGF. In particular, the multicomponent systems exhibited a significant increment of dissolution. These novel systems could be used as alternative matrices in pharmaceutical formulations to improve the bioavailability of ABZ by increasing its solubility and dissolution in SGF and thus optimizing the therapeutic response of ABZ.

ACKNOWLEDGMENTS

Authors wish to acknowledge the assistance of the Consejo Nacional de Investigaciones Científicas y Técnicas (CONICET) and the Universidad Nacional de Córdoba, both of which provided support and facilities for this investigation. Also, project MinCyT-CONICET-CAPES is gratefully acknowledged.

FUNDING

The authors thank the Fondo para la Investigación Científica y Tecnológica (FONCYT) [Préstamo BID PICT 2013-0504], the Secretaría de Ciencia y Técnica de la Universidad Nacional de Córdoba (SECyT), and the Brazilian National Council for Scientific and Technological Development (CNPQ) for financial support.

REFERENCES

1. Bauer JF. Polymorphism: a critical consideration in pharmaceutical development, manufacturing and stability. J Technol. 2008;15–23.
2. Brittain HG. Polymorphism and solvatomorphism 2010. J Pharm Sci. 2012;101(2):464–84. https://doi.org/10.1002/jps.22788.
3. Flórez J. Fármacos antiparasitarios. II. Helmintos y artrópodos. In: Farmacología Humana. Barcelona: Masson S.A.; 1998. p. 1239–47.
4. Barrera MG, Leonardi D, Bolmaro RE, Echenique CG, Olivieri AC, Salomon CJ, et al. In vivo evaluation of albendazole microspheres for the treatment of *Toxocara canis* larva migrans. Eur J Pharm Biopharm. 2010;75(3):451–4. https://doi.org/10.1016/j.ejpb.2010.03.017.
5. García A, Barrera MG, Piccirilli G, Vasconi MD, Di Masso RJ, Leonardi D, et al. Novel albendazole formulations given during the intestinal phase of *Trichinella spiralis* infection reduce effectively parasitic muscle burden in mice. Parasitol Int. 2013;62(6):568–70. https://doi.org/10.1016/j.parint.2013.08.009.
6. Solomon N, Kachani M, Zeyhle E, Macpherson CNL. The natural history of cystic echinococcosis in untreated and albendazole treated patients. Acta Trop. 2017;171:52–7. https://doi.org/10.1016/j.actatropica.2017.03.018.
7. Chattah AK, Zhang R, Mroue KH, Pfund LY, Longhi MR, Ramamoorthy A, et al. Investigating albendazole desmotropes by solid-state NMR spectroscopy. Mol Pharm. 2015;12(3):731–41. https://doi.org/10.1021/mp500539g.
8. Pranzo MB, Cruickshank D, Coruzzi M, Caira MR, Bettini R. Enantiotropically related albendazole polymorphs. J Pharm Sci. 2010;99(9):3731–42. https://doi.org/10.1002/jps.22072.
9. Martinez L, Lamprou DA, McBurney RT, Halbert GW. A novel hot-melt extrusion formulation of albendazole for increasing dissolution properties. Int J Pharm. 2016;499(1-2):175–85. https://doi.org/10.1016/j.ijpharm.2016.01.006.
10. Priotti J, Codina AV, Leonardi D, Vasconi MD, Hinrichsen LI, Lamas MC. Albendazole microcrystal formulations based on chitosan and cellulose derivatives: physicochemical characterization and in vitro parasiticidal activity in *Trichinella spiralis* adult worms. AAPS PharmSciTech. 2017;18(4):947–56. https://doi.org/10.1208/s12249-016-0659-z.
11. Pradines B, Gallard JF, Iorga BI, Gueutin C, Loiseau PM, Ponchel G, et al. Investigation of the complexation of albendazole with cyclodextrins for the design of new antiparasitic formulations. Carbohydr Res. 2014;398:50–5. https://doi.org/10.1016/j.carres.2014.06.008.
12. Chattah AK, Pfund LY, Zoppi A, Longhi MR, Garnero C. Toward novel antiparasitic formulations: complexes of albendazole desmotropes and β-cyclodextrin. Carbohydr Polym. 2017;164:379–85. https://doi.org/10.1016/j.carbpol.2017.01.098.
13. Gurrapu A, Jukanti R, Bobbala SR, Kanuganti S, Jeevana JB. Improved oral delivery of valsartan from maltodextrin based proniosome powders. Adv Powder Technol. 2012;23(5):583–90. https://doi.org/10.1016/j.apt.2011.06.005.
14. Ku R, Sahoo N, Arijit Guha B, Sahoo N, Kuotsu K. Development and in vitro/in vivo evaluation of controlled release provesicles of a nateglinide maltodextrin complex. Acta Pharma Sin B. 2014;4(5):408–16.
15. Zhang J, Zhang X, Wang X, Huang Y, Yang B, Pan X, et al. The influence of maltodextrin on the physicochemical properties and stabilization of beta-carotene emulsions. AAPS PharmSciTech. 2017;18(3):821–8. https://doi.org/10.1208/s12249-016-0572-5.
16. Aiassa V, Zoppi A, Albesa I, Longhi MR. Inclusion complexes of chloramphenicol with β-cyclodextrin and aminoacids as a way to increase drug solubility and modulate Ros production. Carbohydr Polym. 2014;121:320–7. https://doi.org/10.1016/j.carbpol.2014.11.017.
17. Granero GE, Maitre MM, Garnero C, Longhi MR. Synthesis, characterization and in vitro release studies of a new

acetazolamide–HP-β-CD–TEA inclusion complex. Eur J Med Chem. 2008;43(3):464–70. https://doi.org/10.1016/j.ejmech.2007.03.037.
18. Aiassa V, Zoppi A, Albesa I, Longhi MR. Inclusion complexes of chloramphenicol with β-cyclodextrin and aminoacids as a way to increase drug solubility and modulate ROS production. Carbohyd Pol. 2015;121:320–7. https://doi.org/10.1016/j.carbpol.2014.11.017.
19. Mura P, Maestrelli F, Cirri M. Ternary systems of naproxen with hydroxypropyl-β-cyclodextrin and aminoacids. Int J Pharm. 2003;260(2):293–302. https://doi.org/10.1016/S0378-5173(03)00265-5.
20. Higuchi T, Connors KA. Phase-solubility techniques in advances. In: Analytical chemistry and instrumentation, vol. 4. New York: Interscience; 1965. p. 117–212.
21. Moore WJ, Flanner HH. Mathematical comparison of dissolution profiles. Pharm Technol. 1996;20:64–74.
22. Costa P. An alternative method to the evaluation of similarity factor in dissolution testing. Int J Pharm. 2001;220(1-2):77–83. https://doi.org/10.1016/S0378-5173(01)00651-2.
23. Garnero C, Aloisio M, Longhi M. Ibuprofen-maltodextrin interaction: study of enantiomeric recognition and complex characterization. Pharmacol Pharm. 2013;4(01):18–30. https://doi.org/10.4236/pp.2013.41003.
24. Lindenberg M, Kopp S, Dressman JB. Classification of orally administered drugs on the World Health Organization model list of essential medicines according to the biopharmaceutics classification system. Eur J Pharm Biopharm. 2004;58(2):265–78. https://doi.org/10.1016/j.ejpb.2004.03.001.